The 6th International Supercritical CO_2 Power Cycles Symposium
March 27 - 29, 2018, Pittsburgh, Pennsylvania

Characterization of Oxide Scale Structures on Alloys exposed to Open-Fired sCO_2 Power Cycles

Tapasvi Lolla
Engineer/ Scientist III
Electric Power Research Institute
Charlotte, NC

John Shingledecker
Senior Program Manager
Electric Power Research Institute
Charlotte, NC

Steve Kung
Technical Executive
Electric Power Research Institute
Charlotte, NC

Mike Gagliano
Program Manager
Electric Power Research Institute
Charlotte, NC

Ian Wright
Wright HT Inc.
Denver, CO

Adrian Sabau
Senor R&D Staff Member
Oak Ridge National Laboratory
Knoxville, TN

ABSTRACT

In an ongoing effort to predict corrosion/oxidation rates of metallic heat exchangers for open-fired supercritical CO_2 (sCO_2) power cycles, candidate metallic materials were subjected to a series of isothermal laboratory tests in a simulated sCO_2 working fluid at high temperatures and 200-bar pressure. The extent of oxide growth and morphologies of the formed oxide scales were studied using a scanning electron microscope (SEM). Recent advances in SEM detector technology allow for 'closer' examination of the oxide scales using ultra-high resolution imaging capabilities without limitations to the field-of-view, unlike other characterization techniques like TEM. Variations in morphological features of the oxide layers were investigated for five alloys (ferritic-Grade 91, austenitic-304H and TP347H and nickel based 617 and 740H) using such high-resolution imaging techniques. Oxide scale thickness measurements were performed and compared for the five alloys after test durations of 1000, 3500, and 5000 hours, at test temperatures of 700°C. It was found that ferritic and austenitic materials exhibit similar oxide scale features as typically seen when exposed to high temperature steam. In contrast, nickel based alloys show a bimodal scale structure consisting predominately of a sub-micron size uniform single layer with dispersed formations of surface nodules that exhibit a duplex scale structure.

INTRODUCTION

CO_2 based supercritical fluid power cycles are being considered as an alternative to steam based Rankine cycle in heat recovery systems. Pressurized CO_2 as a working fluid for heat exchange is attractive because it may offer numerous advantages over the current steam based systems. Primarily, the relatively low critical pressure of carbon dioxide (7.4 MPa) would allow plant operation while maintaining supercritical conditions throughout the operating cycle, thus eliminating heat loss associated with constant temperature processes such as boiling or condensation. In addition, due to its higher density and volumetric heat capacity, carbon dioxide in its supercritical stage is more energy dense than other working fluids. This may also offer other benefits such as reduction in the size of plant required for a given output and an increased overall cycle efficiency. Higher density of sCO_2 also results in higher airfoil loading and lower cycle pressure ratios across the turbine. Hence, the resulting turbine exhaust has significant remaining enthalpy that can be recovered using recuperators and transferred to the high-pressure fluid. A higher energy-density plant based on sCO_2 power cycles can be realized using compact recuperative and fired heat exchanger designs that are capable of operating at the temperatures and pressures required to attain the desired overall efficiency.

Standard plate-and-tube heat exchanger designs are expected to be too large and cost prohibitive for efficient operation under the pressures and temperatures of proposed sCO_2 power cycles. For this reason, compact recuperator designs that are based on plate matrix, checkerboard and printed circuit configurations are being explored for this application [Le Pierres, 2014]. However, the general dearth of information regarding the performance of typical high temperature alloys in the high temperature and pressure environment of envisioned sCO_2 based plants pose a certain challenge in material section for such components. Furthermore, their complex geometries and the use of thin alloy sections in these compact designs can introduce complications in various stages of their deployment, such as during fabrication. These challenges may include the applicability of joining processes to achieve such complex shapes and ensuring appropriate properties are imparted to the thin alloy sections. One such material property that is critical for their successful application is adequate resistance to corrosion/ oxidation by the working fluid at the operating environment.

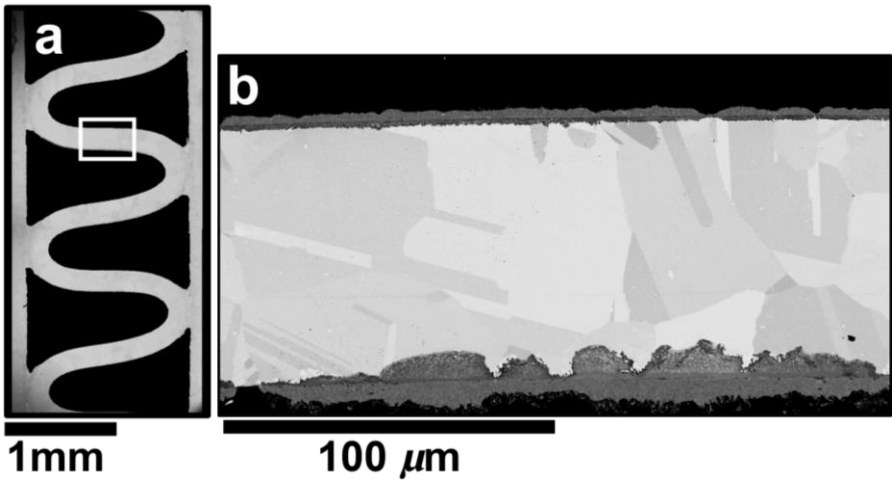

Figure 1: Images of: a) a cross section of a recuperator design showing channels for sCO_2 gas flow; b) magnified cross section image of a thin-section region, as marked in a), showing the formation of oxide scales on the surface.

Based on experience from conventional electric utility plants, it is well known that alloys operating at high steam temperatures form protective oxide scales on surfaces exposed to steam. When the oxide scale reaches a critical thickness, exfoliation events may be triggered during plant start-up or cool down, which can cause blockages in heat exchanger (superheater) tubes [Sabau, 2014, Armitt, 1978]. Since the flow channels in some of the heat recuperator designs intended for sCO_2 plants, will be significantly smaller than typical superheater tubes in a boiler, knowledge of oxide scale growth rate of the alloys chosen for such construction, when exposed to the sCO_2 environment, becomes a crucial factor in the overall alloy selection process.

APPROACH

In a cross-cutting materials project to address oxide scale formation on alloys under sCO_2 conditions, multiple alloys were exposed to a simulated sCO_2 environment at high temperatures, to understand their oxidation behavior. The main objective of the project was to develop computational models to predict the oxidation rate of such alloys in sCO_2 power cycles, which required determining the thickness of oxide scales formed on these alloys after prolonged exposure to impure sCO_2 environment. For this purpose, sections of candidate alloys were introduced into a laboratory test loop with an impure sCO_2 mixture, containing 3.6 vol.% O_2 and 5.3 vol.% H_2O, as a working fluid. The samples were subjected to isothermal tests at 200 bar pressure, for durations of 1000, 3500 and 5000 hours. Oxide scales formed on these tested samples were then examined using a scanning electron microscope. This present work details the characterization studies performed on oxide scales of five alloys (Grade 91, TP304H, TP347H, 617 and 740H), that were isothermally tested at 700°C. Further information regarding the project, including details

of the sCO_2 test mixture, material selection process, testing assembly and test conditions employed, and the development of oxide growth models in sCO_2 conditions, are discussed elsewhere [**Refer to DOE and sCO_2 conference**].

ADVANCES IN SCANNING ELECTRON MICROSCOPY

Scanning electron microscopes (SEMs) have been used as a platform for imaging micron level features in a variety of research fields and in samples ranging from biological tissues to semi-conductor devices. This is mainly because the versatile nature of this machine makes it adaptable to various industries and applications. The SEM can be equipped with a wide range of detectors capable of gathering information that can be useful for imaging, studying compositional variations and quantitative chemical analysis, obtaining structural information and even textural properties of metallic samples. Some of the features and capabilities of the present generation of SEMs are: improved electron sources, in-situ mechanical testing, lithography and 3D imaging. For imaging purposes, the SEM predominantly utilizes signals from secondary electrons (SEs) and backscattered electrons (BSEs) that are emitted from the sample surface upon interacting with the primary electron beam. These signals can be used to gather morphological and compositional information respectively, from topographical and chemical contrast [Vernon-Parry, 2000].

To capture images with high lateral resolution, good control over a number of parameters is essential. These parameters include, beam voltage and beam current, working distance (the distance between the sample and the pole piece), sample preparation, and sample conductivity. In particular, the working distance (WD) is one parameter that can have a large impact on resolution of topographical features. At a larger WD, it is possible to achieve a higher depth of focus. However, the size of the electron probe and beam aberrations increase with WD, which impact the resolution of the image. Hence, imaging at low WDs is important to achieve high resolution images and to capture features that are in the sub-micron range. Unfortunately, conventional SEMs may not be able to capture enough signal (mainly secondary electrons) from the sample at low working distances (below 5mm). This is mainly because the conventional secondary electron detector, also called the Everhart–Thornley detector (ETD), sits at a lateral location from the sample, just below the pole piece, as shown in Figure 2a. Due to the location of this detector in the SEM chamber, at lower working distances, signal from the secondary electrons reaching the detector is insufficient to generate an image with a good contrast. In addition, the location of this detector causes an increase in the signal to noise ratio (noise is considered as secondary electrons: SE_2, SE_3, emitted from other sources in the chamber that reach the detector), which also effects the resolution of the image [Goldstein, 2003].

New annular secondary electron detectors, called in-lens and in-column detectors, were recently introduced in SEM designs [Zhang, 2016]. These in-lens detectors (T1 and T2) are located near the objective lens of the pole piece and the in-column detector (T3) is located in the SEM beam column, as shown in Figure 2b. Researchers have shown that the signal reaching the in-lens detectors have a higher fraction of secondary electrons emitted by the sample (SE_1) due to the primary SEM beam interaction, thus resulting in lower noise [Griffin, 2011]. Furthermore, it has been demonstrated that images generated from in-lens detectors are mainly composed of low energy secondary electrons that are emitted from the near-surface region of the sample, and hence have high surface sensitivity [Kumagai, 2009]. In contrast, the Everhart–Thornley detector receives a larger fraction of electrons with high kinetic energy, which suppress information from low energy electrons originating from the surface, thus leading to loss of sensitivity to surface information.

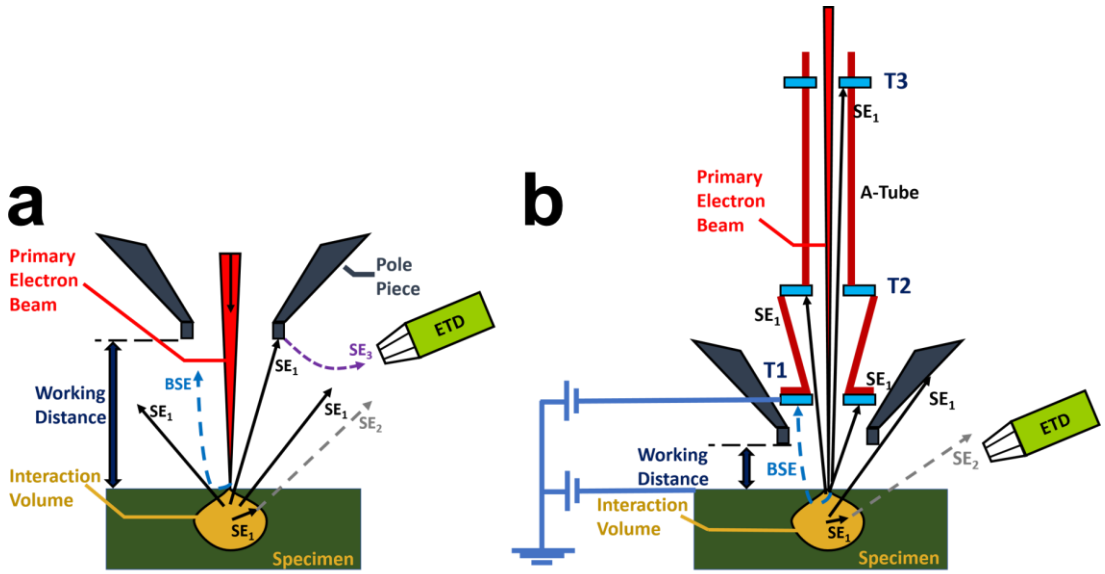

Figure 2: Schematic representation of: a) a conventional microscope and; b) advanced microscope with in-lens and in-column detectors. The schematic also shows the location of Everhart–Thornley detector (ETD), the signals from the specimen resulting from interaction with primary electron beam and the effect of sample working distance on the signals reaching ETD detector

The in-column lens (labeled T3) is located in a flight tube (A-tube) that can be electrostatically biased to accelerate secondary and backscattered electrons from the specimen and enabling them to travel through the length of the tube and reach the detector. Hence, this detector can be used to separate high energy electrons from the signal that reaches T1 and T2 detectors. This also results in improved collection efficiency of the two in-lens detectors, T1 and T2. In addition, due to its location near the pole tip, the T1 detector can capture electrons with relatively large take off angles and, depending on the working distance, can act as a backscattered detector. This combination of detector functionalities and their placement in the SEM enables simultaneous acquisition of topographical and chemical signals from the sample, with enhanced spatial resolution and surface sensitivity. The advantages offered by these new secondary electron detectors were utilized in this work to study the oxide scales formed on the surface of some of the high temperature alloys exposed to sCO_2.

Recent studies have shown that short term exposure of some austenitic and nickel based materials to high temperatures resulted in formation of oxide scale features that were too fine to be resolved using a conventional SEM. For this reason, these oxide features have been studied using alternative, higher resolution techniques, such as scanning transmission electron microscopy (STEM) [Pint, 2017]. Their capability to allow visualization of extremely small features, however, comes at the cost of a very small field of view and time intensive sample preparation. In such instances, the use of these new secondary electron detectors may be advantageous due to simpler sample preparation and the ability to achieve a larger field of view, while not compromising on the resolution required to identify and distinguish various features of such oxide scales.

SAMPLE PREPARATION

After exposure to sCO_2 environment for the pre-determined duration, the tested samples were removed from the testing rig and metallographically prepared for examining the thickness and morphology of their respective oxide scales. For metallurgical examination, the samples were sectioned using a slow-speed high-precision diamond saw in order to minimize any damage to the oxide scale. The sectioned samples were mounted in a high edge-retention conductive epoxy to prevent material loss at the edges of the sample during sample polishing. Mounted samples were then prepared using standard metallurgical

polishing practice, which involved multiple, successively finer abrasive polishing stages. Abrasive polishing was continued until the samples attained a surface finish of 0.5 µm. For the final stage of polishing, the samples were transferred to a vibratory polisher, which imparted a surface finish of 0.05 µm. Polished samples were cleaned using alcohol and baked in an oven to remove any organic residue. Using a scanning electron microscope with in-lens detectors, investigations were carried out to study the oxide scale structures on the polished samples. The results from these investigations are presented in the following section.

RESULTS AND DISCUSSION

The morphology and thickness of oxide scales formed on each of the five alloys after 1000, 3500 and 5000 of exposure to sCO_2 environment were determined using SEM-based techniques.

Exposure of Grade 91 alloy to sCO_2 at 200 bar and 700°C

Figure 3 shows a combined backscattered and secondary electron images of the oxide scale formed on Grade 91 steel, when exposed to sCO_2 at 700°C after 1000, 3500 and 5000 hours (Figures 3a, 3b and 3c respectively). The oxide scale was found to be relatively uniform in thickness and appeared to consist of three distinct layers. This observation is in contrast to the two-layered structure typically found on Grade 91 after exposure to steam in a conventional plant [Wright, 2011]. The innermost layer (L1) exhibited a banded (or laminated) structure, with the bands running parallel to the L1-alloy interface, and in general appeared to have significant fine porosity. The overall morphology of L1 appeared very similar to that formed in high-pressure steam atmosphere [Wright, 2011], where the inner layer was identified as Fe-Cr rich spinel structure (magnetite containing Cr). The outer oxide scale, designated as L2, appeared to consist of two distinct layers. The morphology of the inner L2 layer was consistent for all exposure times and exhibited a large columnar-grained structure, typical to that found after steam exposure, where the columnar layer was found to be magnetite (Fe3O4). In addition, this layer exhibited distributed porosity, which appears to increase with increasing test duration. To study the distribution of elements in the three different layers, elemental distribution maps were generated from energy dispersive spectroscopy (EDS) analysis of the oxide scale.

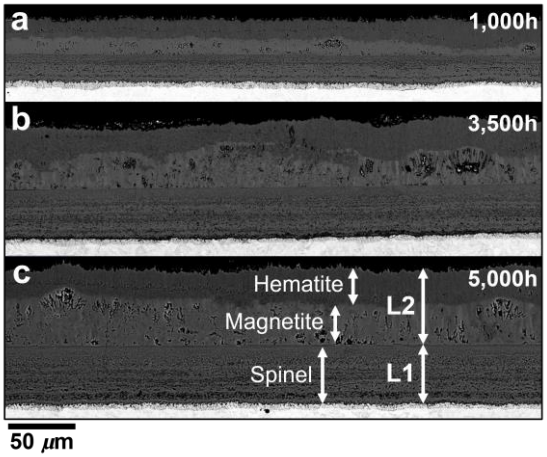

Figure 3: SEM images from cross-sections of Grade 91, showing the oxide scale formed after exposure for 1,000, 3,500, and 5,000 hours at 700°C to CO_2 containing 3.6 vol.% O_2 and 5.3 vol.% H_2O at 200 bar.

Figure 4a shows a backscattered electron image of a cross section of the scale formed on Grade 91, along with EDS elemental maps of the same area for Fe, Cr, and O (Figures 4b, 4c and 4d respectively). The scale had a well-delineated layered structure with a Cr enriched L1 layer and a relatively Cr-free outer L2 layer. Within the L1 layer, areas of Cr enrichment were apparent in successive laminates, particularly for laminates close to the interface with the alloy. This indicated that the L1 layer consisted of successive layers

of Fe-rich magnetite and Cr-rich spinel layers, similar to that seen in steam environment. Oxygen tracer studies suggest that L1 grows predominantly by inward transport of gaseous CO_2 through L2, and that new oxide forms throughout the thickness of L1, rather than solely at the L1-alloy interface [Taylor, 1980]. Similarly, the two distinct regions in L2 appeared to have a difference in oxygen concentration, with the outer L2 layer having a higher oxygen concentration. This trend was consistent for all exposure times and suggested that L2 layer consisted of a relatively lower-oxygen containing magnetite layer and a higher-oxygen concentration hematite. The growth of L2 involves outward transport of iron ions and formation of new magnetite at the L2-gas interface. It is possible that, over time, L1-alloy interface may become enriched with Cr (most often by transport along alloy grain boundaries) so that the overall transport of reactants slows, and the reduced outward flow of iron ions allows hematite to develop at the L2- sCO_2 interface.

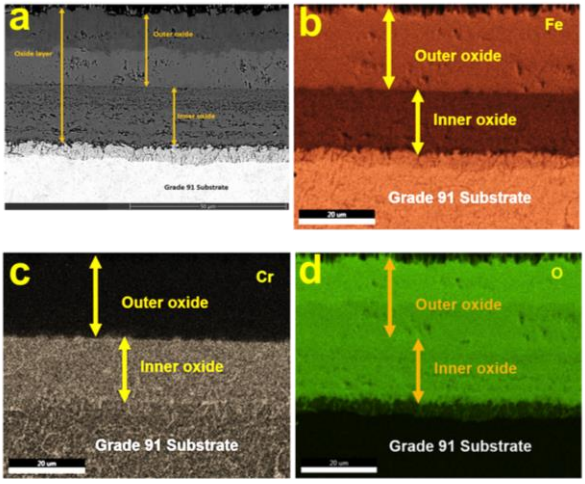

Figure 4: a) SEM image and corresponding EDS maps of: b) Fe; c) Cr; d) O, at the oxide scale formed on Grade 91 at 700°C after exposure to CO_2 containing 3.6 vol.% O_2 and 5.3 vol.% H_2O at 200 bar.

Oxide scale measurements were performed to understand the rate of oxide growth on Grade 91 material; Figure 5 shows a typical example of the measurements performed. The resulting total oxide thicknesses after 1,000 and 3,500, and 5,000h are presented in the box normal plot shown in Figure 6.

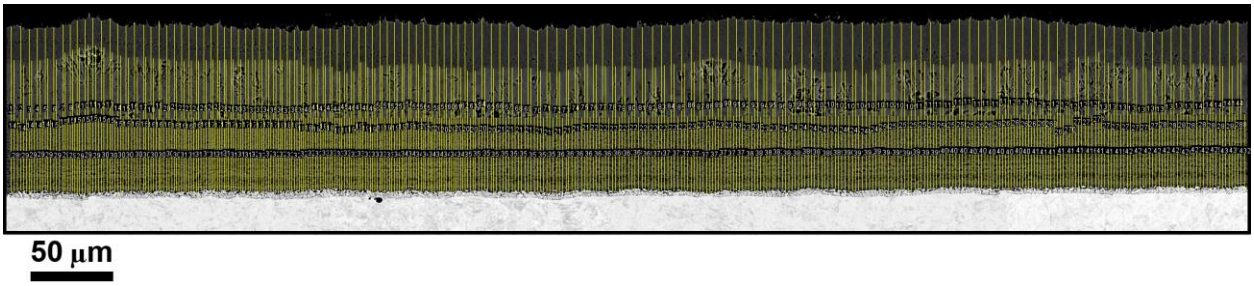

Figure 5: Image showing an example of oxide scale measurements on a backscattered electron image of a cross-section of Grade 91 oxide scale, formed after exposure at 700 °C to CO_2 containing 3.6 vol.% O_2 and 5.3 vol.% H_2O at 200 bar.

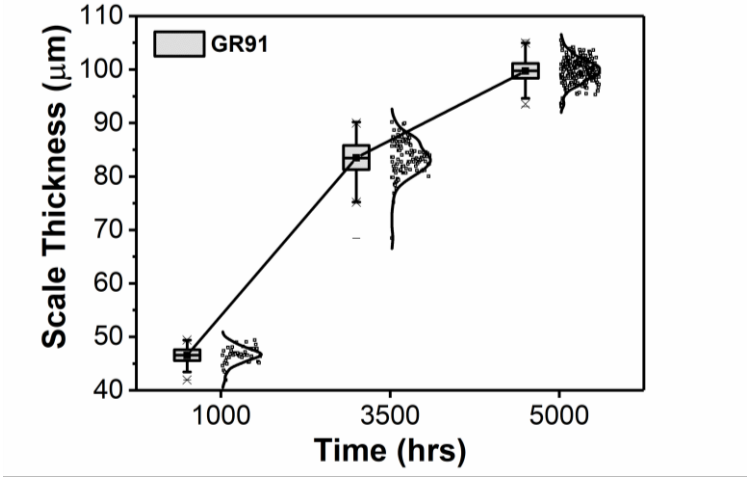

Figure 6: Box normal plot showing the total scale thicknesses formed on Grade 91 after exposure at 700°C for up to 5,000 hours, in CO_2 containing 3.6 vol.% O_2 and 5.3 vol.% H_2O at 200 bar

From the graph, Grade 91 displays a near normal distribution of the oxide scale measurements for all exposure durations. This implies that the oxide scale is uniform at all tested conditions, suggesting a uniform growth behavior of the different oxide layers. The rate of oxidation was found to be larger for the initial exposure duration of 1000 hours (approximately 0.047 μm/ hour), and reduced gradually for the subsequent exposure durations of 3500 hours (approximately 0.025 μm/ hour) and 5000 hours (approximately 0.02 μm/ hour). This trend is consistent with the parabolic rate of growth for oxide scale that has been observed in Grade 91 material exposed to high-pressure, high temperature steam environment [Wright, 2011].

Exposure of TP304H alloy to sCO_2 at 200 bar and 700°C

Images of the oxide scale formed on austenitic TP304H material from exposure to sCO_2 conditions after the three exposure durations at 700°C are shown in Figure 7. The oxide scale formed after each of the three exposures consisted of a duplex structure, similar to those formed in high-pressure steam environments [Wright, 2011]. In all the three instances, the thickness of the inner layer (L1) was extremely irregular, whereas the thickness of the outer layer (L2) was relatively uniform. As in the case of the inner oxide layer in Grade 91 steel, the inner layer of oxide in TP304H appears to show a lamellar structure. However, unlike Grade 91, the laminates are irregular in shape and do not appear to be parallel to the alloy-L1 boundary. In addition, they do not seem to be continuous due to the formation of nodule like structures. These nodules did not exhibit any obvious features (such as banding or a definite grain structure in L1), but appear to contain scattered oxide particles intermixed with bright–appearing islands of metallic particles and voids. The L2 consists of large columnar grains growing perpendicular to the L1-L2 interface that seem to become smaller, more equiaxed and contain more distributed porosity with increasing distance from the L1-L2 interface. In addition, a semi-continuous band of voids was present seemingly along the L1-L2 interface. Occurrence of such voids is typical of what is commonly found in steam-formed scales, and ultimately where separation of L2 from L1 eventually occurs.

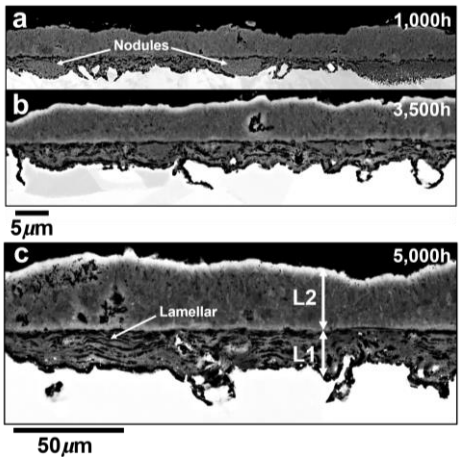

Figure 7: SEM images from cross-sections of TP304H, showing the oxide scale formed after exposure for 1,000, 3,500, and 5,000 hours at 700°C to CO_2 containing 3.6 vol.% O_2 and 5.3 vol.% H_2O at 200 bar.

An SEM image and corresponding EDS elemental maps for Fe, Ni, Cr, and O are shown in Figure 8a-e, respectively, for a section of the scale formed after 3,500h. The SEM/BSE image indicates that in addition to its non-uniform thickness, L1 generally consists of multiple layers. The elemental maps did not provide further discrimination of this scale structure, except that there was some enrichment in Cr along the L1-alloy interface, similar to scale formed in steam. While there were no obvious Cr-rich precipitates in the alloy, areas of nickel enrichment in L1 appears to coincide with the isolated islands of alloy substrate, particularly near the alloy-L1 interface. It is postulated that during oxidation of austenitic steels (such as TP304H) in high-pressure steam, Ni is rejected (as metal) near or ahead of the oxidation front, resulting in discrete islands of intact metal. The features shown in Figures 7 and 8a suggest that the process by which L1 forms in sCO_2 with oxidizing impurities is similar to the L1 formation in steam. The elemental maps in Figure 8 suggest that L2 is essentially of uniform composition, and most likely comprised of magnetite.

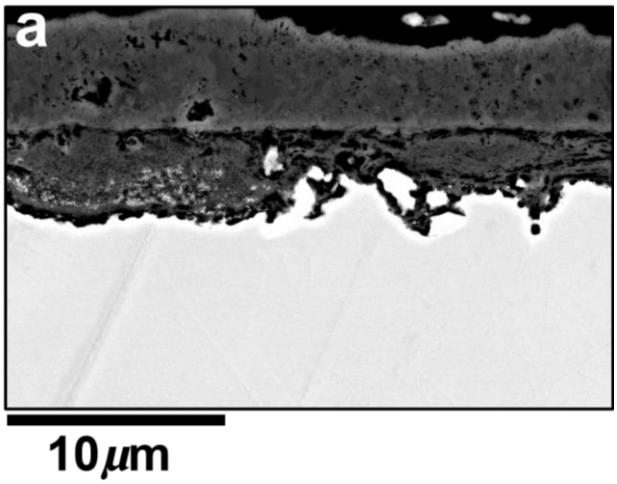

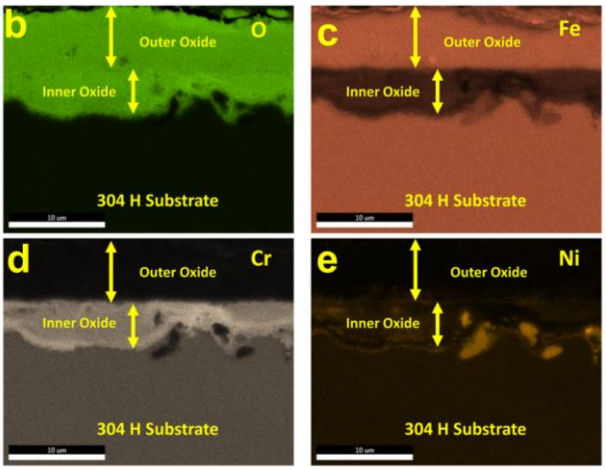

Figure 8: SEM image of a cross section of scale formed on TP304H after exposure to sCO_2 for 3,500 hours at 700°C, 200 bar, and corresponding EDS maps of: a) O; b) Fe; c) Cr; d) Ni, at the oxide scale.

Thickness of the oxide scale formed on TP304H after exposure to sCO_2 atmosphere after different durations was measured and the resulting measurements were plotted as shown in Figure 10. From the graph, the oxide scale formed after 1000 and 3500 hours of exposure appears to have a bimodal nature. However, after 5000 hours of exposure, the oxide thickness shows a near normal distribution. This may be because of a combination of irregular L1 layer thickness and a progressive increase in the relative thickness of the larger, and more uniform, L2 layer.

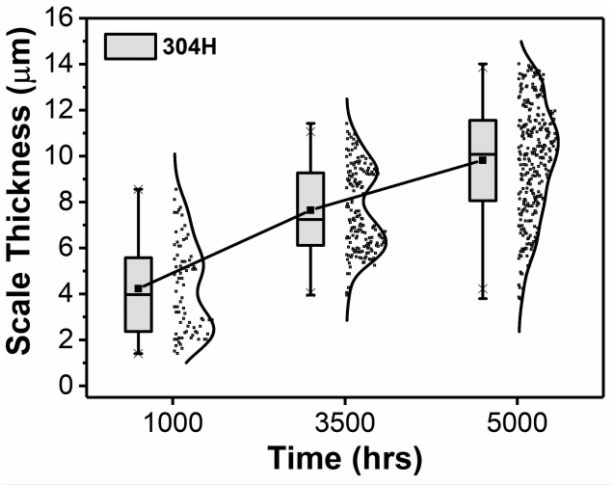

Figure 9: Box normal plot showing the total scale thicknesses formed on TP304H after exposure at 700°C for up to 5,000 hours, in CO_2 containing 3.6 vol.% O_2 and 5.3 vol.% H_2O at 200 bar.

Exposure of TP347H alloy to sCO_2 at 200 bar and 700°C

The morphology of the oxide scales formed on TP347H at 700°C in a sCO_2 environment after different exposure times, are shown in Figure 10. Although after 1000 hours in sCO_2 conditions, the oxide scale formed on TP347H has a duplex oxide structure (L1 and L2), the thinness of the oxide scale made it difficult to distinguish the individual layers. After 3,500 hours, the dual nature of the oxide scale in TP347H is more evident. Similar to the morphology of scale in TP304H, the inner oxide layer (L1) also exhibits a non-uniform and discontinuous lamellar appearance. The L2 layer on the other hand displays a columnar grain structure, similar to the L2 layer of TP304H. The TP347H sample tested for 5000 hours also exhibits

similarities in scale morphology with that of TP304H. Nodules in the L1 layer were clearly evident, along with the columnar grain structure of L2 scale. To quantify the thickness of the oxide scale formed on the TP347H samples, and to compare the oxide growth behavior with TP304H, oxide scale measurements were performed. The results of the analysis are shown in Figure 12.

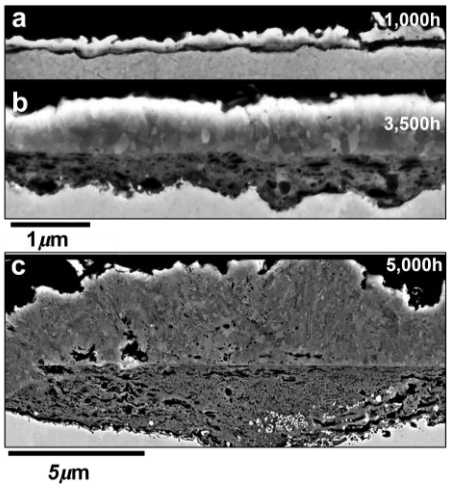

Figure 10: SEM images from cross-sections of TP347H, showing the oxide scale formed after exposure for 1,000, 3,500, and 5,000 hours at 700°C to CO_2 containing 3.6 vol.% O_2 and 5.3 vol.% H_2O, at 200 bar.

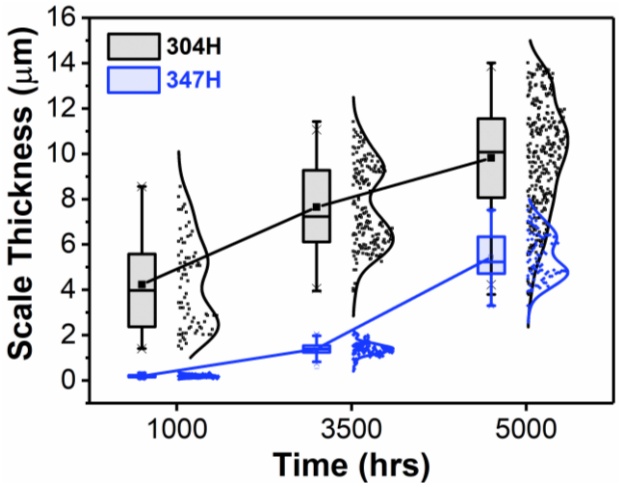

Figure 11: Box normal plot showing the total scale thicknesses formed on TP304H and TP347H after exposure at 700°C for up to 5,000 hours, in CO_2 containing 3.6 vol.% O_2 and 5.3 vol.% H_2O at 200 bar.

Relative to the oxide scale thickness of TP304H material after 1000 hours, which generally was between 2 to 4 µm, the measured oxide scale thickness on TP347H was less than 0.5 µm. After 3500 hours of exposure the oxide scale formed in sCO_2 environment was typically 1 to 1.5 µm in total thickness, which was approximately six times lower than that formed on TP304H under similar conditions (6 to 9 µm). After 5000 hours in sCO_2 environment, the oxide scale thickness on TP347H ranged between 4.5 to 6.5 µm, which was about half the scale thickness formed on TP304H (8 to 12 µm). In general, the rate of oxidation of TP347H, was found to be markedly slower than that of TP304H

Exposure of IN617 alloy to sCO_2 at 200 bar and 700°C

Figure 12 shows SEM images of the scales formed on IN617 after 1,000, 3,500, and 5,000 hours exposure. These images are a result of advanced in-lens detection capability of an SEM. After 1,000 hours of exposure, the scale formed was non-uniform in thickness and consisted of a random distribution of single layer and duplex (dual-layered) oxide with associated porosity; larger double-layered nodules were also present in some locations. Compared to the scale structure after 1,000 hours, the scale formed after 3,500 hours of exposure appeared to be predominately double-layered with a few areas where it was much thinner and consisted of a single layer. Both layers were non-uniform in thickness, with the inner L1 layer typically thicker than the outer L2 layer. L1 layer also appeared to contain significant porosity in the form of large voids, whereas L2 appeared to have a columnar-grained structure. After 5,000 hours in the sCO_2 environment, the scale formed on IN617 at 700°C appeared to have developed morphological features similar (but much thinner) to those typically found on austenitic steels. That is, two layers in which the thickness of L1 was irregular and L2 was relatively uniform. However, unlike austenitic steels, there were select regions where the scale was thinner and single-layered. In the example shown in Figure 13c, L2 appears to consist of columnar grains that span the whole layer thickness. However, the structure within L1 is was difficult to determine.

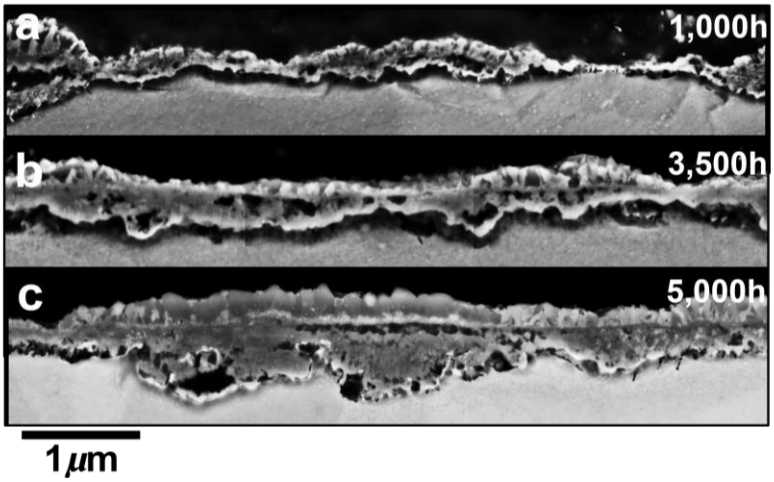

Figure 12: SEM images from cross-sections of IN617, showing the oxide scale formed after exposure for 1,000, 3,500, and 5,000 hours at 700°C to CO_2 containing 3.6 vol.% O_2 and 5.3 vol.% H_2O at 200 bar.

In the absence of prior information or approach for systematically determining whether the scale was single or multi-layered, for measurement purposes only the total thickness was considered. The measurements made are summarized in the box plot graph in Figure 13, which demonstrated a large variability in the thickness of these very thin scales.

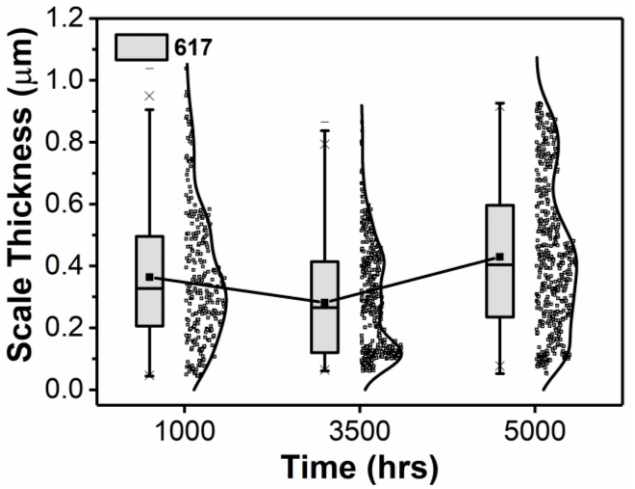

Figure 13: Box normal plot showing the total scale thicknesses formed on IN617 after exposure at 700°C for up to 5,000 hours, in CO_2 containing 3.6 vol.% O_2 and 5.3 vol.% H_2O at 200 bar.

Exposure of IN740H alloy to sCO_2 at 200 bar and 700°C

SEM images of oxide scales formed on IN740H in an impure sCO_2 environment after different durations of exposure, are shown in Figure 14. After 1,000 hours, the scale appeared to consist of a single layer oxide with uniform thickness. Such a structure is quite comparable with earlier observations (using lower-resolution optical microscopy) that scales formed on this alloy in high-pressure steam were mostly thin and featureless, with isolated thicker nodules and penetrations into the alloy surface [Wright, 2009]. In the oxide sublayer, the presence of fine precipitates is evident, which may be associated with a specific phase, possibly γ'. The scale formed after 3,500 hours at 700°C was mostly double-layered, with a few sporadic regions where the scale was thinner and single-layered. Most regions of L1 appeared featureless and free of pores, while L2 had a well-defined columnar-grained structure and the variations in brightness within the L2 layer suggest that the composition was non-uniform. Overall, the scale morphology was reminiscent of that formed on austenitic steel TP304H, but on a much finer scale. The absence of chemical analysis precluded the drawing of further parallels with the mode of scale development formed on TP304H. After 5,000 hours of exposure, the scale appeared thinner than that observed after 3,500 hours, and a much smaller section of the scale exhibited a double-layered structure. L1, present either as a single layer or an inner layer, appeared to be featureless and, in some areas, voids were apparent at the L1-L2 interface.

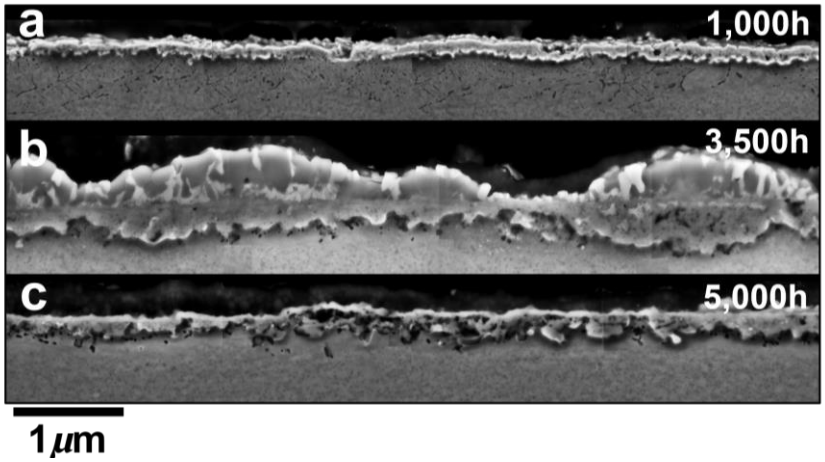

Figure 15: SEM images from cross-sections of IN740H, showing the oxide scale formed after exposure for 1,000, 3,500, and 5,000 hours at 700°C to CO_2 containing 3.6 vol.% O_2 and 5.3 vol.% H_2O at 200 bar.

Measurements of total scale thicknesses on IN740H are displayed in Figure 16. A comparison of thickness measurements between the different exposure durations shows much greater scatter after 3,500 hours, and its effect on the statistical representation of thicknesses. Although the oxide scale on both IN617 and IN740H

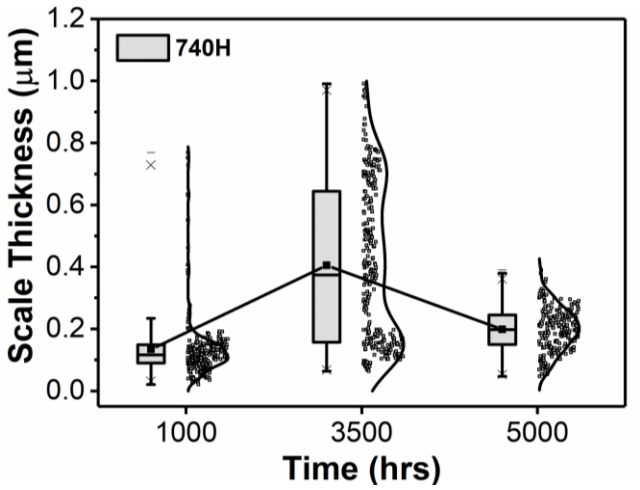

Figure 6: Box normal plot showing the total scale thicknesses formed on IN740H after exposure at 700°C for up to 5,000 hours, in CO_2 containing 3.6 vol.% O_2 and 5.3 vol.% H_2O at 200 bar.

SUMMARY

- The morphology and thickness of oxide scales formed on five high temperature alloys, when exposed to sCO_2 environment at 700°C and 200 bar, was determined using a new-generation of high-resolution scanning electron microscope with in-lens and in-column detectors.
- This work highlights the advantage of such high-resolution electron microscopes over other imaging techniques such as STEM, in obtaining information from a larger field of view, while not compromising on the resolution of the image.
- Oxide scale measurement techniques were developed with an aim of capturing the variability in the oxide scale thickness and morphology.
- Grade 91 alloy was found to have a uniform three-layered oxide scale, with a lamellar inner oxide layer similar to that observed in high-pressure steam environment, and the two outer layers of the scale are believed to be magnetite and hematite.
- Both the austenitic stainless steel alloys (TP304H and TP347H), displayed a duplex oxide scale structure, wherein the inner oxide displayed a non-uniform and irregular lamellar structure, and outer oxide was uniform with columnar grains.
- The overall rate of oxide growth on TP347H was found to be markedly lower than that formed on TP304H for similar exposure duration and conditions.
- The oxide scales formed on the two nickel based alloys (IN617 and IN740H) were less than 1μm at all tested durations
- Due to the very thin nature and complex morphology of the oxide scale formed on the four austenitic alloys, there was significant variation in the measured thickness of the total oxide scale. This highlights the difficulty in modeling the oxidation phenomenon and oxide growth behavior of these alloys.

REFERENCES

Armitt, J., Holmes, D.R., Manning, M.I., Meadowcroft, D.B. and Metcalfe, E., "The Spalling of Steam-Grown Oxide From Superheater and Reheater Tube Steels, EPRI Report No. FP-686, Feb (1978).

Goldstein, J., Newbury, D.E., Joy, D.C., Lyman, C., Echlin, P.E., Lifshin, E., Sawyer, L. & Michael, J., "Scanning Electron Microscopy and X-ray Microanalysis", 3rd ed. New York, NY: Kluwer Academic/Plenum Publishers, (2003)

Griffin, B.J., "A comparison of conventional Everhart- Thornley style and In-Lens secondary electron detectors: A further variable in scanning electron microscopy". Scanning 33, 162–173, (2011).

Kumagai, K., Sekiguchi, T., "Sharing of secondary electrons by In-Lens and outlens detector in low-voltage scanning electron microscope equipped with immersion lens", Ultramicroscopy 109, 368–372, (2009).

Kung, S., Shingledecker, J., Wright, I., Lolla, T., and Sabau, A, "Corrosion of Heat Exchanger Alloys in Open-Fired sCO2 Power Cycles", Proceedings of 6th International Supercritical CO_2 Power Cycles Symposium, Pittsburgh, Pennsylvania, March 27 - 29, (2018).

Le Pierres, R., Southall, D., and Osborne, S., "Impact of mechanical design issues on printed circuit heat exchangers," Supercritical CO_2 Power Cycle Resource Center (2014).

Pint B. A., Unocic, K. A., Brese, R. G. & Keiser, J. R., "Characterization of chromia scales formed in supercritical carbon dioxide", Materials at High Temperatures, 35:1-3, 39-49, (2017)

Sabau, A.S., Wright I.G., Shingledecker J.P., and Tortorelli, P.F., "Managing oxide scale exfoliation in boilers with TP347H superheater tubes," Proceedings of 7th International Conference on Advances in Materials Technology for Fossil Power Plants, Waikoloa, Hawaii. EPRI (2014).

Shingledecker, J., Kung, S. and Wright, I., "Predicting the Oxidation/Corrosion Performance of Structural Alloys in Supercritical CO_2", DOE Award Number: DE-FE0024120, Final Technical Report, (2017)

Taylor, M.R., Calvert, J.M., Lees, D.G. and Meadowcroft, D.B., "The mechanism of corrosion of Fe-9%Cr alloys in carbon dioxide," Oxidation of Metals, 14 (6), 499-516, (1980).

Wright, I.G. and Dooley, R.B., "Morphologies of oxide growth and exfoliation in superheater and reheater tubing of steam boilers," Materials at High Temperatures, 28 (10), 40-57 (2011).

Wright, I.G., DOE FWP No. FEAA061: Oxidation of Candidate Alloys in Steam at 17 bar—Final Report on Phase 1 Efforts in Support of the U.S. Consortium Program on Boiler Materials for Ultra-Supercritical Coal Power Plants, ORNL/TM-2009/232, Nov. (2009)

Vernon-Parry, K.D. "Scanning electron microscopy: An introduction". III-Vs Rev. 13, 40–44, (2000)

Zhang, X., Cen, X., Ravichandran, R., Hughes, L. A., van Benthem, K., "Simultaneous Scanning Electron Microscope Imaging of Topographical and Chemical Contrast Using In-Lens, In-Column, and Everhart-Thornley Detector Systems", Microscopy and Microanalysis, Jun;22(3):565-75 (2016)

ACKNOWLEDGEMENTS

The samples used in this study were obtained from work supported by the Department of Energy under Award Number DE-FE0024120. Neither the United States Government nor any agency thereof, nor any of their employees, makes any warranty, express or implied, or assumes any legal liability or responsibility for the accuracy, completeness, or usefulness of any information, apparatus, product, or process disclosed, or represents that its use would not infringe privately owned rights. Reference herein to any specific commercial product, process, or service by trade name, trademark, manufacturer, or otherwise does not necessarily constitute or imply its endorsement, recommendation, or favoring by the United States Government or any agency thereof. The views and opinions of authors expressed herein do not necessarily state or reflect those of the United States Government or any agency thereof.